Pergamon

Int. J. Heat Mass Transfer. Vol. 37, No. 10, pp. 1441–1453, 1994

0017-9310/94 $7.00 + 0.00

0017-9310(93)E0098-2

Flow and heat transfer regimes during quenching of hot surfaces

Y. BARNEA and E. ELIAS
Department of Mechanical Engineering, Technion—Israel Institute of Technology, Haifa, Israel

and

I. SHAI
Department of Mechanical Engineering, Ben-Gurion University, Beer-Sheva, Israel

(*Received* 5 *January* 1993 *and in final form* 24 *November* 1993)

Abstract—An experimental and theoretical study of flow and heat transfer regimes during quenching of a heated vertical channel is presented. The objective of the experimental portion of the research was to obtain quantitative data and observations on the reflooding of an annular channel typical to small research reactors. Data were used to assist the formulation of a theoretical model to predict the rate of precursory cooling during reflooding. Tests were carried out at constant inlet pressure using subcooled water as a working fluid. Measurements included inlet and outlet flow conditions, vapor and liquid temperatures along the test section and the volumetric void fraction as a function of distance from the quench front. Surface heat flux was calculated from the fast temperature measurements along the heated surface. The quench front is shown to lie in the transition boiling region which spreads into the dry and wet segments of the surface.

1. INTRODUCTION

THE PROCESS of quenching of hot surfaces is important in light water reactor accident analysis, cryogenic heat transfer, metallurgy and in the oil, gas and chemical processing industries. For instance, a hypothetical loss of coolant accident (LOCA) in water cooled nuclear reactors may result in rapid heating of the fuel channels. In order to prevent the fuel from reaching a metallurgically prohibitive temperature, a low pressure injection system (LPIS) is activated at a predetermined reactor pressure or coolant level. The activation of the LPIS marks the beginning of the reflooding phase of the accident. The initial fuel rods temperature, in this phase, may be greater than the rewetting temperature, which is the highest temperature at which a direct contact is possible between the fuel cladding and the coolant. The subcooled coolant flow, under such conditions, is known as a post-dryout two-phase flow. It is characterized by the formation of a wet patch on the hot surface which eventually develop into a moving quench front.

As the quench front progresses along the flow channel, it removes heat from the hot surface by several heat transfer mechanisms such as axial conduction and radial convection and radiation to the coolant. Two types of flow regimes may exist downstream of the quench front. At high inlet velocities the dominant flow regime is the inverted annular flow (IAF) in which a liquid core flows at the center of the channel surrounded by a vapor annulus. At lower inlet flow rates an inverted slug flow (ISF) regime typically prevails. In both cases, the two-phase mixture downstream of the quench front acts as a precursory heat sink, which gradually decreases the surface temperature prior to quenching. With the increase in the vapor quality downstream of the quench front, the flow pattern changes to dispersed flow (DF) and eventually to single-phase vapor flow.

Numerous theoretical and experimental studies on the heat and mass transfer mechanisms during top and bottom reflooding have been reviewed by Yadigaroglu [1], Elias and Yadigaroglu [2], Collier [3] and Olek [4]. Freon is often used as a working fluid to simulate the high pressure quenching of a BWR or PWR fuel channel [5–7]. The stability and flow characteristics of the IAF regime has been the subject of many studies in the last two decades. Using a γ-densitometer to measure the void fraction distribution in liquid nitrogen flowing in a vertical tube, Ottosen [8] observed a transition from the IAF to a dispersed droplet flow at a void fraction of 0.8. A visual photographic analysis of an idealized single phase core inverted annular flow has been reported by Ishii and Denten [9] using a freon-113 jet surrounded by a coaxial annulus of nitrogen gas. A transition from IAF to ISF and DF was also observed by Goodman and Elias [10] and Edelman *et al.* [11] for water at atmospheric pressure.

Careful examination of the available precursory cooling heat transfer data during reflooding reveals that while an extensive data base is available on the flow structure far from the quench front region, not

NOMENCLATURE

A	cross sectional area
C	heat capacity
C_p	liquid heat capacity at constant pressure
d	wall thickness
D_h	hydraulic diameter of heated tube
G	mass flux
g	gravity
k	thermal conductivity
k'	thermal conductivity
h	heat transfer coefficient
L	heated length
L_δ	length of vapor film
Nu	Nusselt number
Pe	Peclet number
Pr	Prandtl number
q''	surface heat flux
R	outer radius of heated tube
r	radius
Re	Reynolds number
T	temperature
t	time
U	velocity
y	radial coordinate
Z	distance from inlet plane
z	axial coordinate.

Greek symbols

α	thermal diffusivity
β	thermal expensivity
δ	vapor film thickness
ε	thermal emissivity
μ	viscosity
$\bar{\mu}$	liquid film thickness
ρ	density
ψ	dimensionless parameter, equation (2)
σ	Stefan–Boltzmann coefficient.

Subscripts

AR	apparent rewetting
g	vapor
IB	incipient boiling
in	inlet conditions
l	liquid
max	maximum heat flux
q	quench front
r	rewetting
rad	radiation
s	saturation conditions
sub	subcooling
tr	transition
w	heated wall.

many studies deal with the complex transport phenomena taking place at the quench front itself. As a result of the objective difficulties in measuring heat and flow parameters near the quench front [12, 13], there is currently no conclusive description of the prevailing heat transfer regimes at that region. Moreover, recent experimental data are reported mainly for heated vertical tubes or rods bundle which simulate LOCA conditions in PWR and BWR (e.g. [14, 15]) while data in other flow configurations, relevant to experimental and test reactors, are scarce.

The main motivation of the experimental portion of this research was to obtain experimental data and observations on the reflooding of an annular channel with initial wall temperature below 600°C and low inlet flow rates, typical to small research reactors. The data were used as a basis for a mechanistic theoretical model for predicting the heat and mass transfer at the quench front and along the precursory cooling region. The model uses a multizone thermohydraulic approach to predict the heat transfer coefficient at the quench front during bottom reflooding with subcooled liquid.

This article is based on a broader thesis research [16], which describes the experiments and modeling in detail. The portion of the experiments that offer new and unique results and those results that are necessary for the model development are presented.

2. EXPERIMENTAL SET-UP AND PROCEDURE

The experimental facility, shown schematically in Fig. 1, consists of a peripheral loop and a test section. The peripheral loop includes a centrifugal pump, a filtering unit, a preheater and a pressurized filling vessel. The pressure in the filling vessel provides a constant upstream pressure for the centrifugal pump, and basically defines the initial inlet water velocity. The inlet flowrate varied significantly during the initial period of the test due to the expected variations in the frictional and acceleration back-pressure in the test section. A quasi-steady state was gradually reached in a later phase of the test as the quench front progresses along the channel.

Analysis and data reduction were based on measurement taken when the quench front had reached the upper part of the test section near thermocouple No. 2 (located 657 mm below the top of the test section). At that point the quench and inlet velocities were almost stable and the end effects (due to slow top quenching) are minimal. All experiments were performed at atmospheric static pressure in the test section which was practically open to the ambient at its exit.

The test section, Fig. 2, consists of an electrically heated inconel-600 tube with wall thickness 2.4 mm and an effective heated length of 800 mm. The tube is

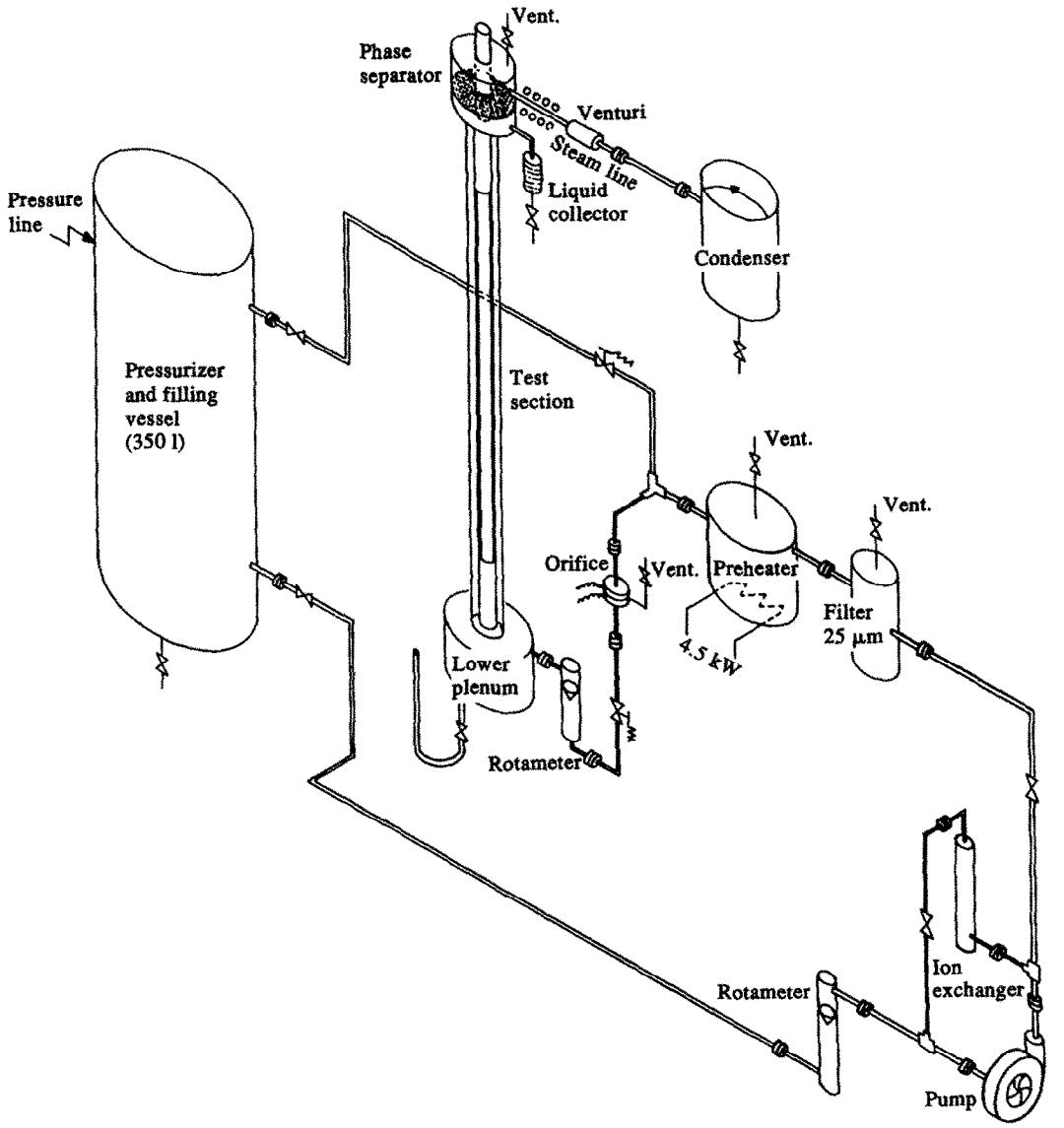

FIG. 1. Schematic of experimental facility.

located at the center of a larger quartz pipe (wall thickness 3 mm) forming an annular flow channel whose dimensions are 44.8 mm i.d. and 54 mm o.d. corresponding to the outer tube diameter and the inner quartz diameter respectively. The test section is attached to a lower plenum and a separator at its inlet and outlet planes, respectively.

The tube temperature is measured by twelve 0.5 mm$^{\phi}$ ungrounded K type thermocouples which are inserted through the inner surface of the tube and soldered into the metal at five elevations along the heated section. At certain elevations along the tube, several thermocouples were installed at different azimuthal angles in order to detect azimuthal non-uniformities in the quench front zone. An additional ten bare thermocouples (No. 30) were inserted through the external glass tube, at five different elevations, to measure the liquid and vapor temperature along the flow channel.

A specially designed phase separator is applied at the channel's outlet to allow for a direct verification of the mass and energy balance in the test section. It consists of a thermally insulated double-wall vessel which collects and separate the two-phase flow mixture exiting from the top of the test section. To avoid condensation of the two-phase mixture during the experiment, the outer separator's wall temperature is kept slightly above saturation by applying electric heating tapes. Measurements of the exit vapor and the liquid carryover flows are performed by continuously draining and weighting the liquid phase. The vapor phase is first superheated slightly and accelerated through the upper outlet of the separator, and then condensed and continuously weighted.

A stationary γ-densitometer using 300 mCi ^{241}Am isotope (γ energy of 60 keV) and a 5 × 5 cm cylindrical NaI(Tl) scintillation detector was applied to measure the void fraction non-intrusively in the vicinity of

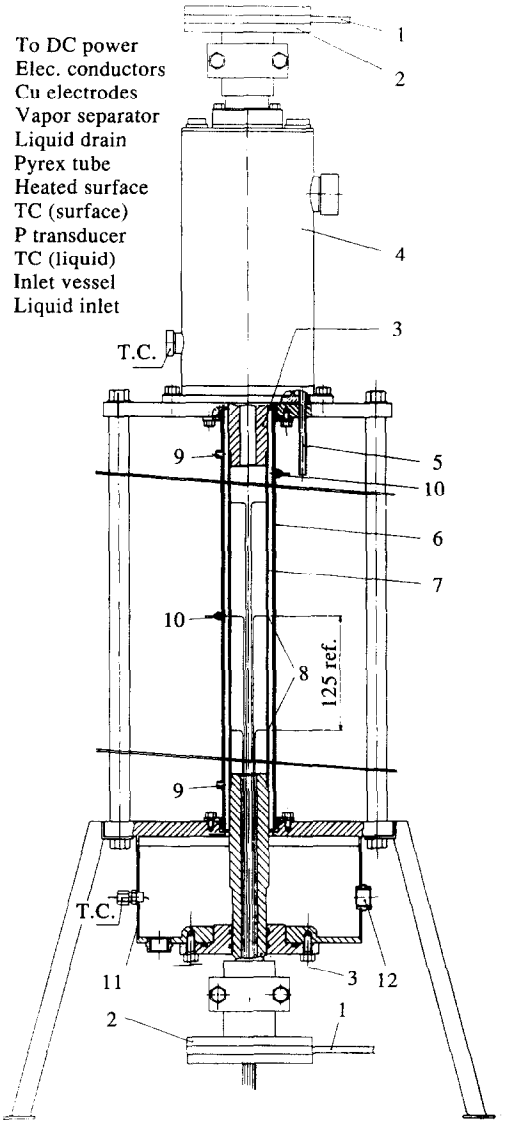

FIG. 2. Sketch of the annular test section with the inlet chamber at the bottom.

the quench front. The densitometer utilizes a narrow beam which is directed tangential to the outer surface of the heated tube. With proper calibration, the density measurement also enables the evaluation of the vapor film thickness at the heated wall, as outlined in ref. [11].

The test procedure consists of heating the inconel tube electrically (using 30 kVA stabilized DC power supply) to a predetermined temperature while keeping the test section in an inert (Ar gas) or steam environment. The inert gas is injected through a special valve in the water inlet chamber at the bottom of the channel and is pushed out through the vapor exit by the vapor generated at the early phase of the test. During the initial heat-up process, the quartz pipe is cooled to about 50°C by forced circulation of air through a series of nozzles located along its outer surface. During the test, the quartz tube's temperature remains almost unchanged. This procedure ensures that no boiling and vapor generation takes place at the inner quartz surface during the test. Heat losses to the environment through the glass are generally small (of the order of 50 W m^{-1}) having only negligible effect on the heat balance over the quench zone (heat rate at the quench front is of the order of 50 kW m^{-1}).

3. RESULTS AND DISCUSSION

The experimental program covers the range of parameters of interest for research reactors analysis including five feed vessel absolute pressures in the range of 0.1 to 0.5 bar, six initial tube temperatures in the range of 350 to 600°C and two inlet water temperatures; 30 and 60°C (70 and 40°C subcooling, respectively). Recorded data include: surface temperatures at 5 different elevations and 2 azimuthal positions along the test section; fluid temperatures at 5 axial locations; time variation of the void fraction at a fixed level (measured by the γ-ray densitometer); pressure difference along the coolant flow channel; flow rates of the inlet water, exit steam and the liquid carryover; and inlet and exit water temperatures and exit steam temperature. Data were recorded as a function of time starting when the bottom thermocouple (located 3.2 cm above the inlet) is quenched.

A few tests were repeated for consistency checks. Some of the runs were video taped to enable better visualization. A total of 46 runs with complete data sets are available. Some of the data are presented in this section according to the physical phenomena they describe.

3.1. *Quench front velocity*

The prediction of the quench front velocity has been the main goal of many theoretical investigations [2, 4, 17]. Theoretical models for this problem involve the solution of the one-dimensional or two-dimensional Fourier heat conduction equation in the solid for specified boundary conditions, representative of the heat transfer processes at the surface. Almost all models use the surface heat transfer coefficient and the rewetting temperature as input parameters, although the need to specify the heat transfer coefficient *a priori* was sometimes eliminated by considering the rewetting problem as a conjugate heat transfer problem [18]. Simultaneous measurements of the quench front velocity along with the heat transfer coefficient and the rewetting temperature are presented here which could serve as a data base for model validation.

The quench front velocity is calculated from the measured wall temperatures. A sample of the wall temperature histories is shown in Fig. 3 for two initial wall temperatures, 400 and 575°C, and two inlet water temperatures, 30 and 60°C. The temperature–time curves obtained in five thermocouples located at equal distances (125 mm) along the upper section of the inconel tube are shown. In all the curves the wall temperature changes gradually at the early phase of

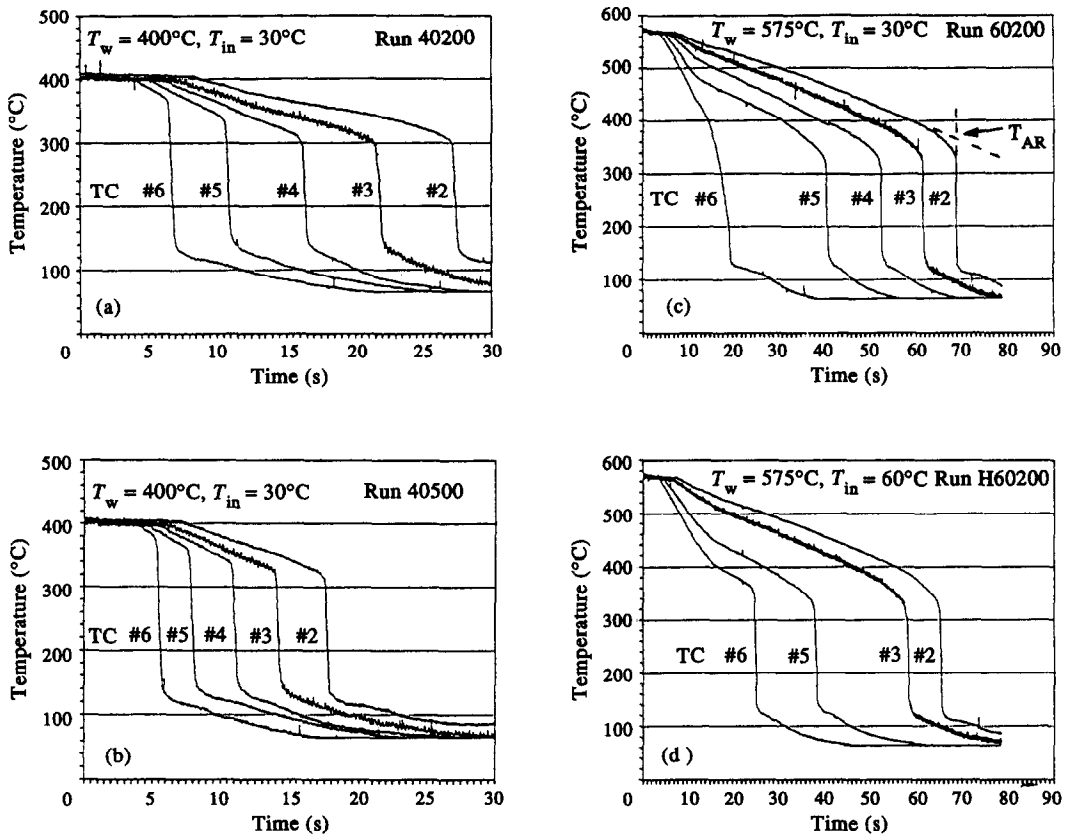

FIG. 3. Surface temperatures vs time for different inlet and initial conditions.

the transient due to early cooling by steam and two-phase mixture produced at the lower part of the tube. At a given elevation the gradual decrease of the wall temperature continues until it quenches, at which time the wall temperature drops sharply to almost a steady value corresponding to the local fluid temperature.

Examination of the results in Fig. 3 shows that the time required for the quench front to reach a specific elevation along the heated tube (quenching time) depends on the initial wall temperature and on the inlet water conditions. The quench front velocity in the vicinity of thermocouple No. 2 is plotted in Fig. 4 using data from four different runs. It is shown that while the quench front velocity varies slightly as the quench front moves along the channel, the ratio between the quench front velocity and the instantaneous inlet water velocity, U_q/U_{in}, remains almost constant during the test. In the present range of conditions, this ratio was found to vary between 0.2 and 0.8 depending on the initial surface temperature and on the inlet water temperature.

Quench front velocity data measured when the quench front has reached thermocouple No. 2 are listed in Table 1 along with the initial wall temperature, T_w, the instantaneous inlet flow velocity, U_{in}, and the inlet water temperature, T_{in}. For comparison, Table 1 lists predictions by the models suggested by Piggot and Duffey [19] and by Edelman *et al.* [11]. Piggot and Duffey's correlation expresses the quench front velocity as a function of the inlet mass flow rate and subcooling but does not account for the initial wall temperature. Their correlation over-predicts the data, sometimes by more than 100%. Edelman's correlation yields satisfactory results for the high wall temperature and high inlet velocity and subcooling cases which are within its suggested range of validity. At lower wall temperatures and lower inlet velocities the data are generally under-predicted.

3.2. *The rewetting temperature*

The local wall temperature at the quench front is important for theoretical modeling of the rewetting problem. There has been some confusion in the literature concerning the exact definition of this parameter manifested in the variety of synonyms used to identify it, such as quench, sputtering, minimum film boiling, Leidenfrost temperature etc., which do not always represent the same physical phenomenon. In this study, the approach of Gunnerson and Yackle [20] is adopted which distinguishes between a quench front temperature and a rewetting temperature. The quench temperature, termed here as apparent rewetting temperature (T_{AR}), is defined at the intersection between the tangent line to the temperature–time curve (or the equivalent curve of temperature vs axial distance) at the point where its slope is the largest, with the tangent to the curve before quenching (cf. Fig. 3). T_{AR} marks the onset of a rapid surface cooling caused by an

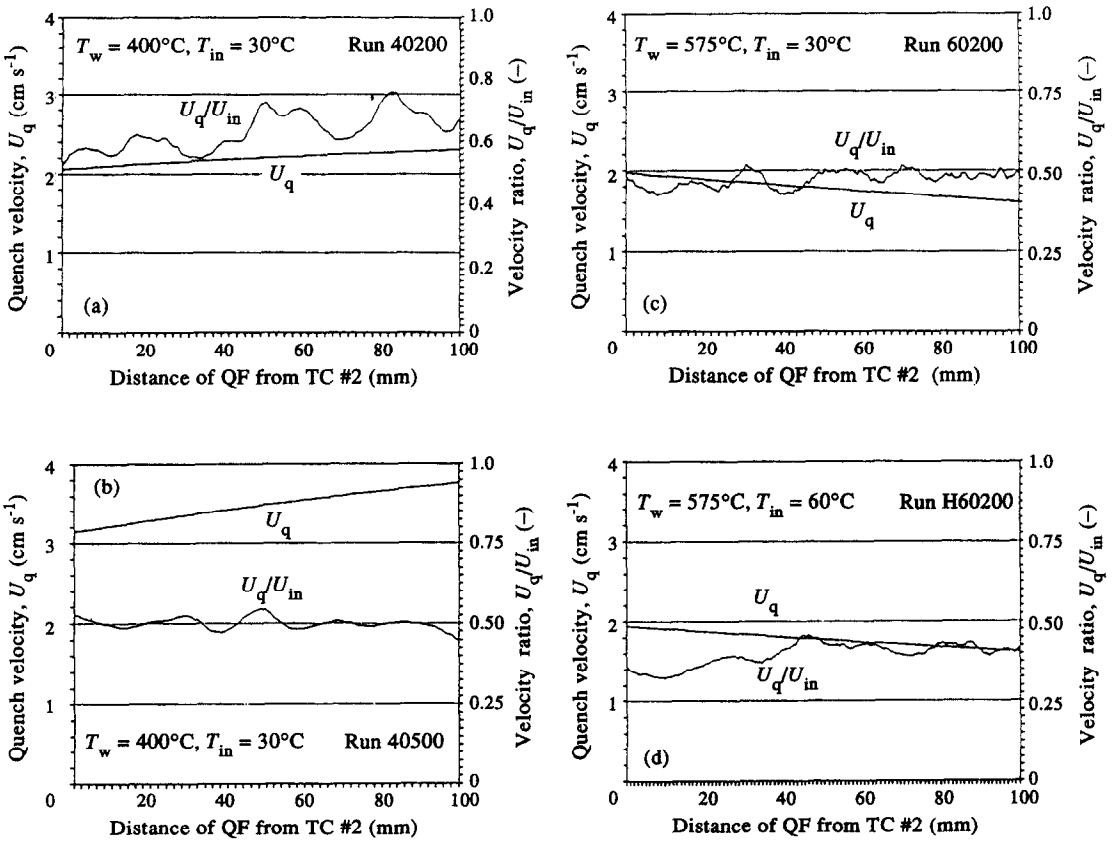

FIG. 4. Quench front velocity and ratio of quench to inlet velocities vs distance from thermocouple number 2.

enhanced rate of heat transfer that does not necessitate liquid–solid contact. The rewetting temperature, on the other hand, is the temperature at which a triple interface, gas–liquid–solid, is formed. This temperature is difficult to define from the measured temperature–time curve. In this study it is taken as the highest temperature at which the slope of the surface temperature vs time curve first exceeds an arbitrary value of 500°C s^{-1} [21].

Apparent rewetting temperatures established by the intersection of tangent lines to the 'knee' of the measured temperature–time trajectories are correlated by Kim and Lee [22] as a function of the wall properties, wall initial temperature and the coolant inlet temperature and mass flux, G.

$$\frac{T_{AR}-T_s}{T_w-T_s}=19.51\left(\frac{T_s-T_{in}}{T_w-T_s}\right)^{0.107}\left[\left(\frac{Cd}{k}\right)_w G\right]^{-0.162}$$

Table 1. Measured and predicted quench front velocities

Exp. *	T_w (°C)	T_{in} (°C)	U_{in} (cm s^{-1})	U_q [meas.] (cm s^{-1})	U_q [predicted] (cm s^{-1}) ref. [11]	U_q [predicted] (cm s^{-1}) ref. [19]
40100†	400	30	2.1	1.5	0.8	2.1
40200	400	30	3.6	2.1	1.5	4.1
40300	400	30	5.0	2.4	2.1	5.1
50200	525	30	3.8	2.0	1.3	3.8
60100	575	30	2.7	1.5	0.8	2.2
H60100‡	575	60	1.8	1.4	0.5	2.6
60200	575	30	4.1	1.8	1.5	2.2
H60200	575	60	4.4	1.8	1.6	4.7
60300	575	30	5.9	2.2	1.7	3.4
H60300	575	60	7.6	1.9	2.2	7.4
60500	575	30	9.0	2.5	2.7	5.1
H60500	575	60	7.4	1.9	1.9	8.6

†Exp. * indicates the initial T_w (400°C) and initial filling vessel pressure (100 kPa).
‡The "H" preceding the Exp. * denotes low inlet subcooling (T_{in} = 60°C).

$$\times\left[\left(\frac{k\rho^2}{d}\right)_w \frac{T_w - T_s}{G^3}\right]^{-0.0989}\left(\frac{Z}{d}\right)^{-0.163} \quad (1)$$

where k, ρ and C are the wall conductivity, density and specific heat respectively, d is the wall thickness and Z is elevation. Equation (1) was found to predict the measured T_{AR}, in thermocouple number 2 ($Z = 657$ mm), within $\pm 10\%$.

Rewetting of the hot surface occurs when a contact is established between the solid and the liquid film adjacent to it. Thus the rewetting temperature can be described as an interface temperature of two suddenly contacting materials. The instantaneous interface temperature of two suddenly contacting bodies has been commonly determined from the solution of the Fourier heat equation. Assuming the wall prior to rewetting to be at temperature T_{AR} and the liquid at T_l, then the rewetting temperature, T_r is given by [23]

$$T_r = \frac{T_{AR} + T_l\sqrt{\psi}}{1+\sqrt{\psi}} \quad (2)$$

where ψ is the ratio between the liquid and the wall properties, $(k\rho C_p)_l/(k\rho C)_w$.

Equation (2) implies that the rewetting temperature varies linearly with the surface temperature prior to quenching, represented by T_{AR}. This behavior was also observed qualitatively by Yu [24] and by Edelman *et al.* [11]. Results by equation (2) are compared in Fig. 5 to the measured rewetting temperatures defined as the surface temperature at which the slope of the temperature–time curve reaches 500°C s^{-1}. In Fig. 5 the liquid properties were calculated at $T_l = 90$°C which was the measured average bulk temperature at the quench zone. Equation (2) predicts the measured rewetting temperature within better than ± 10°C over the entire range of the present experimental conditions.

3.3. *Void fraction and vapor film thickness*

Void fraction data downstream of the quench front are of crucial importance for understanding the precursory cooling mechanisms. Fast photography of the quench region indicated the existence of a vapor film

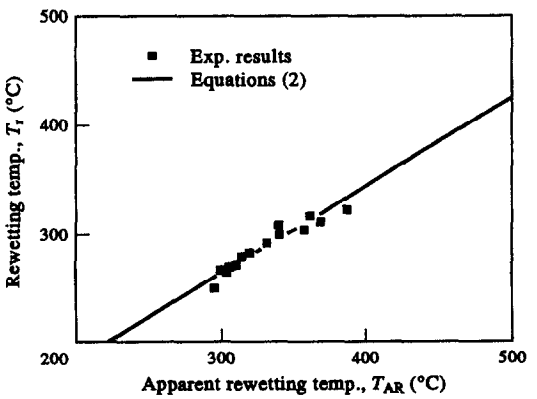

FIG. 5. Rewetting vs apparent rewetting temperatures.

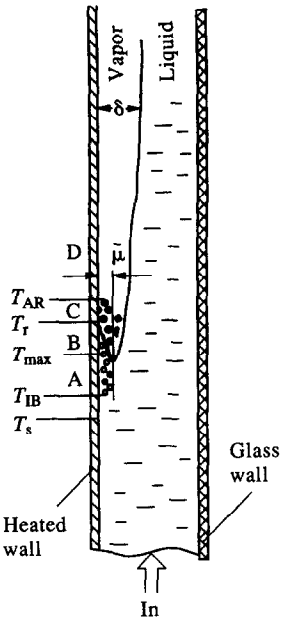

FIG. 6. Schematic of the flow structure near the quench front.

above the quench front, separating the heated surface from the liquid film flowing along the quartz pipe. In all tests the vapor film extended well upstream of the quench front as shown schematically in Fig. 6. The quench front itself consists of a wavy liquid film surrounding the central tube and flowing in an oscillatory manner along the heated wall. The waviness of the quench front was also detected by monitoring the surface temperature at a given elevation using two thermocouples installed at the same elevation but at opposite azimuthal angles (0 and 180°). Note that, in Fig. 6, T_{AR} is located downstream of the rewetting temperature, in accordance with the typical results depicted in Fig. 3. In the wall region bounded between T_{AR} and T_r the heated surface is probably cooled by small liquid droplets impinging on it without forming a continuous film.

Quantitative void fraction and vapor film thickness data are shown in Fig. 7 as functions of the distance from the quench front. The γ-densitometer used in this measurement was located at a fixed position (532 mm above the channel inlet plane) and measurements were carried out as a function of time, every 0.1 s, as the quench front progressed towards it. Thus, the axial distance in Fig. 7 indicates the distance of the quench front below the measurement point. The typical relative error in the void fraction measurements, caused by the statistical nature of the radioactive source, are $\pm 1.5\%$.

Two observations are noted about the data in Fig. 7. First the void fraction at the quench front itself (axial distance of 0 mm) is always greater than 0. This is consistent with the schematic description of the quench region depicted in Fig. 6, indicating that the vapor film indeed extends upstream of the quench front. In other words, the establishment of a solid–

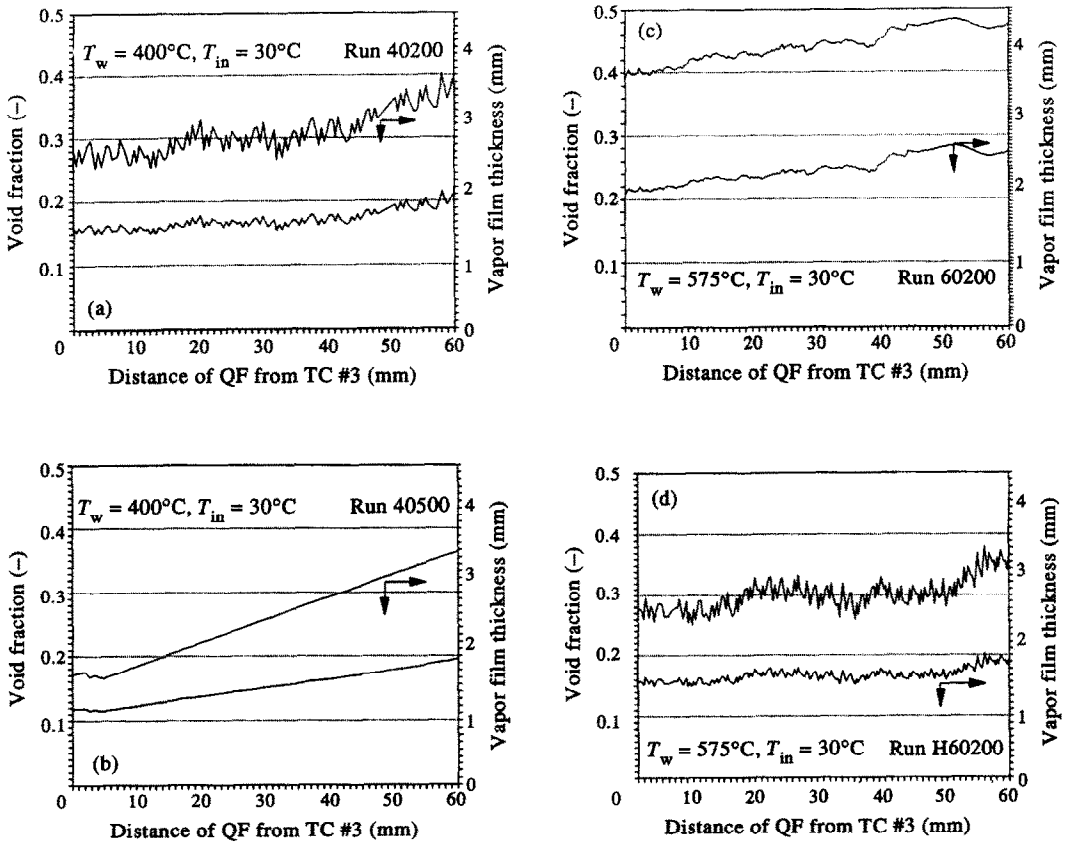

FIG. 7. Void fraction and vapor film thickness along the heated surface for different inlet and initial conditions.

liquid contact at the quench front is not necessarily accompanied by a complete collapse of the vapor film. Moreover, in the first 20–40 mm downstream of the quench front, the vapor film thickness is almost constant (1–2 mm) and then increases monotonically with the distance from the quench front. Similar IAF configurations were observed qualitatively by Goodman and Elias [10] and Obott and Ishii [25] who noticed a smoothed flow section downstream of the quench front. The development and configuration of the vapor film in the IAF regime, shown in Fig. 7, cannot be explained by a Bromely type film boiling. These observations must be included in any phenomenological model of the heat transfer mechanisms at the quench region.

Table 2 lists some important data measured at the quench front region and in the IAF precursory cooling zone. The length, L_δ, and the thickness, δ, of the vapor film in the constant-thickness region are indicated along with the instantaneous inlet velocity, U_{in}, and the local bulk temperature, T_l, at the quench front. Note that the fluid near the quench front is always subcooled. The degree of subcooling at the quench front is proportional to the inlet velocity and decreases with increasing the inlet water temperature. The liquid remains subcooled in the entire smooth region downstream of the quench front. The length of the smooth region depends inversely on the inlet flowrate. This is mainly because increasing the inlet flowrate increases the vapor generation and the vapor film velocity at the quench front. Higher vapor film velocity induces Helmholtz instabilities which eventually break the film. These observations are in agreement with Obot and Ishii [25] who have indicated that, for large gas Weber number, the length of the smooth flow section depends inversely on the gas velocity. The vapor film thickness in the smooth flow section is almost unaffected by the inlet or local conditions.

3.4. *Heat transfer coefficients*

At the quench front, the heat transfer pattern changes within a short distance from a single-phase

Table 2. Typical experimental results in the precursory cooling zone

Exp. *	U_{in} (cm s^{-1})	T_l (°C)	δ (mm)	L_δ (mm)
40200	3.4	95	1.5	35
40300	5.6	92	1.3	30
40400	6.2	90	1.3	21
40500	7.6	80	1.1	5
50200	2.8	90	1.8	40
60200	2.7	83	1.9	45
H60200	2.9	93	1.6	40
60500	5.7	40	1.7	10
H60500	5.7	65	1.4	10

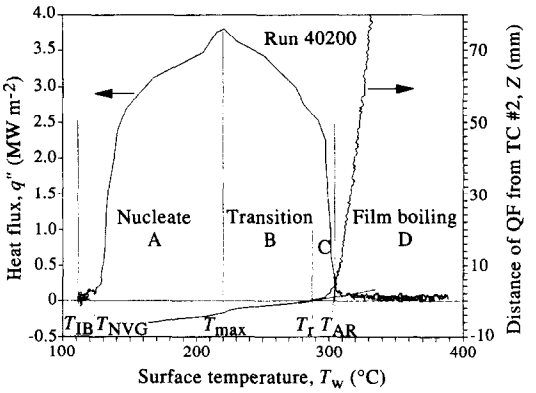

FIG. 8. Heat flux distribution and heat transfer regimes near the quench front.

liquid convective heat transfer via nucleate and transition boiling into a film boiling regime [26]. Since the surface heat transfer coefficient near the quench front cannot be measured directly it was derived from a heat balance. To this end a one-dimensional (axial) time-dependent analysis was applied to a small section of the tube

$$k_w \frac{\partial^2 T}{\partial x^2} - \frac{q''_w}{d} = (\rho C)_w \frac{\partial T}{\partial t} \tag{3}$$

where q''_w is radial heat flux. Equation (3) was solved numerically for the surface heat flux, q''_w, at each time step of the measurement using the recorded temperature–time curves to calculate the temporal and spatial derivatives. Figure 8 is a sample of the calculated heat flux for Run 40200 with initial wall temperature of 400°C, inlet water temperature of 30°C and initial inlet velocity 9.3 cm s^{-1}. The figure presents the heat flux and the wall temperature at the quenching time of thermocouple No. 2 (elevation 657 mm). Positive axial distances on the left axis of Fig. 8 denote distances downstream of the quench front in the dry zone while negative axial distances correspond to points upstream of the quench front in the wet region. Note that the quenching process occurs within a narrow axial region of less than 10 mm. The heat flux at the quench front reaches, in this case, a maximum of about 3.7 MW m^{-2}. This is about twice the maximum heat flux expected in forced convection systems under similar conditions. The maximum heat flux value is obtained upstream of the quench front in the wetted region. The trend presented in Fig. 8 is typical to all the present tests, although, as is explained in the following, the exact shape of the heat flux curve depends on the initial and inlet conditions.

The surface heat flux curve in Fig. 8 covers several heat transfer mechanisms. The heat transfer regimes and characteristic temperatures are also indicated schematically in Fig. 6. Data evaluation enables the definition of four heat transfer zones as follows.

Zone A—Forced convection in subcooled boiling liquid defined along the surface in the temperature interval $T_{IB} < T_w < T_{max}$, where T_{IB} and T_{max} are the onset of boiling temperature and the temperatures at the maximum heat flux point, respectively.

Zone B—Transition Boiling phase-1, is defined along the wetted surface in the temperature interval $T_{max} < T_w < T_r$.

Zone C—Transition Boiling phase-2, which prevails in a small region close to the quench front in the temperature interval $T_r < T_w < T_{AR}$.

Zone D—Subcooled inverted annular film boiling, downstream the quench front, in the dry surface area.

Figure 9 shows the measured heat flux distribution at the quench front region for four different runs. Note that higher rewetting temperatures are measured for higher initial wall temperatures in accordance with equation (1). Also, increasing the liquid inlet velocity increases the maximum heat flux released at the quench front. For wall temperature of 400°C the heat flux increases from 4 MW m^{-2} for initial inlet velocity of 9.3 cm s^{-1} to about 5.5 MW m^{-2} at inlet liquid velocity of 13.5 cm s^{-1}. Varying the inlet subcooling from 40 to 70°C increases the maximum heat flux from 5 to 6 MW m^{-2}.

In this section, the typical heat transfer regions and characteristic temperatures indicated schematically in Figs. 6 and 8 are modeled in order to enable a quantitative derivation of a complete heat transfer coefficient curve applicable for subcooled quenching of hot surfaces.

3.4.1. *Subcooled boiling, zone A.* For surface temperatures below the incipient boiling limit, T_{IB}, heat transfer is predominantly by mixed convection to subcooled liquid. In this region, the following correlation suggested by Collier [27, p. 141] was found to fit the present data with good accuracy.

$$Nu = 0.17 Re^{0.33} Pr_l^{0.43} \left(\frac{Pr_l}{Pr_w}\right)^{0.25} \left[\frac{D_h^3 \rho_l^2 g \beta \Delta T}{\mu_l^2}\right]^{0.10} \tag{4}$$

where the flow Reynolds number, Re, and Nusselt number are determined using the channel hydraulic diameter, D_h. Generally, mixed convection heat transfer upstream of the quench front accounts for only a few percent of the total heat flux during reflooding.

Subcooled nucleate boiling prevails at wall temperatures above T_{IB}. For atmospheric pressure, T_{IB} is given by [28]

$$(T_w - T_s)_{IB} = 0.022 (q''_w)^{0.463} \tag{5}$$

where the temperatures are in °C and q''_w in W m^{-2}.

Equation (5) was solved for T_{IB} and for the heat flux at the onset of boiling point, $(q''_w)_{IB}$, using the measured heat flux vs temperature data (e.g. Fig. 8). In the range of parameters studied in this work, T_{IB} is between 105 and 115°C. The next characteristic temperature in Fig. 8 is the net vapor generation point, T_{NVG}. This point lies at a distance of about 10 mm upstream of the quench front. Characteristic values

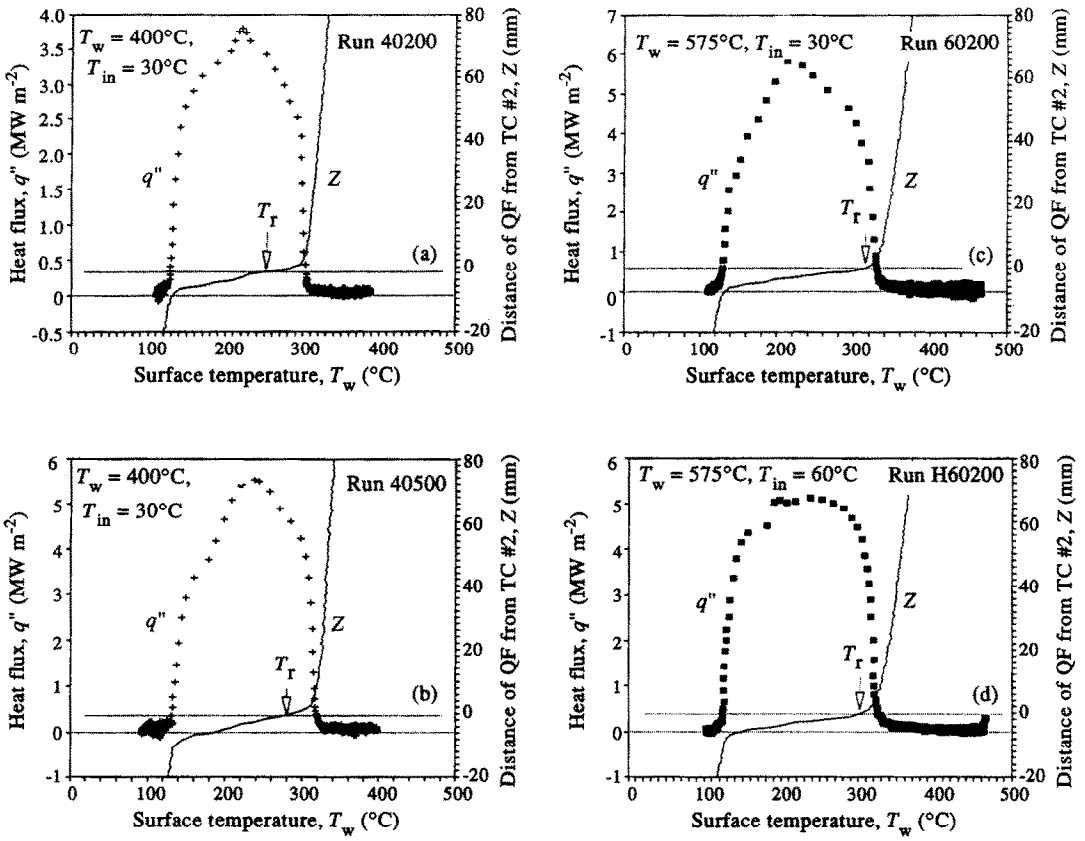

FIG. 9. Heat flux distribution and quench front location vs surface temperature for different inlet and initial conditions.

of T_{NVG} were calculated by applying the correlation derived by Saha and Zuber [29] to the measured heat flux curves. In the present range of measurement, the average liquid bulk temperature at the NVG was found to vary between 60 and 90°C.

In the temperature range between T_{NVG} and the maximum heat flux temperature, T_{max}, the surface heat flux is best represented by the nucleate boiling heat transfer correlation derived by Klimenko [30], which for atmospheric pressure could be represented by

$$q''_w = 424(\Delta T)^{2.5} \quad (6)$$

where q''_w is in W m^{-2} and ΔT in °C. Equation (6) applies for the conditions of the present tests in which the convective boiling number, N_{CB}, is always less than 1.6×10^4.

Good prediction of the wall heat flux ($< \pm 5\%$) is obtained by equation (6) for surface temperatures of less than about 140°C. At higher wall temperatures, intense vapor generation close to the quench front, which is not accounted for in Klimenko's model, reduces the measured heat flux and increases the deviation from equation (6).

The maximum heat flux at atmospheric pressure is affected by the local degree of subcooling. The surface superheat at the maximum heat flux point were, therefore, correlated as

$$\Delta T_{max} = 120 + 0.1 \frac{(k\rho C^2)_w}{(k\rho C_p^2)_l} \Delta T_{sc} \quad (°C) \quad (7)$$

where the wall properties are calculated at the apparent rewetting temperature. Equation (7), which is similar to the correlation developed by Carbajo [31] for water in a stainless-steel pipe, fits the present data within $\pm 5\%$. For saturated flow ($\Delta T_{sc} = 0$) equation (7) predicts a wall superheat of 120°C, which is higher by about 70°C relative to pool boiling data. The maximum heat flux temperature lies upstream of the quench front in the wetted region. It marks the end of the nucleate boiling regime and the onset of transition boiling. Referring to Fig. 6, T_{max} lies between T_s and T_r.

3.4.2. *Transition boiling, zone B.* In region *B* (Fig. 8), which extends in the temperature range $T_{max} < T_w < T_r$, heat transfer is mainly by low quality transition boiling in which nucleate boiling and film boiling alternate on the hot surface; the phenomena are quite similar to those encountered in pool boiling [32]. This zone is characterized by a gradual decrease in the frequency of liquid/surface contacts, and, respectively, by an exponential decrease of the surface heat transfer coefficient with the surface superheat [33]

$$h_B = h_{B,max} \exp\left(\frac{T_{max} - T_w}{T_{max} - T_s}\right). \quad (8)$$

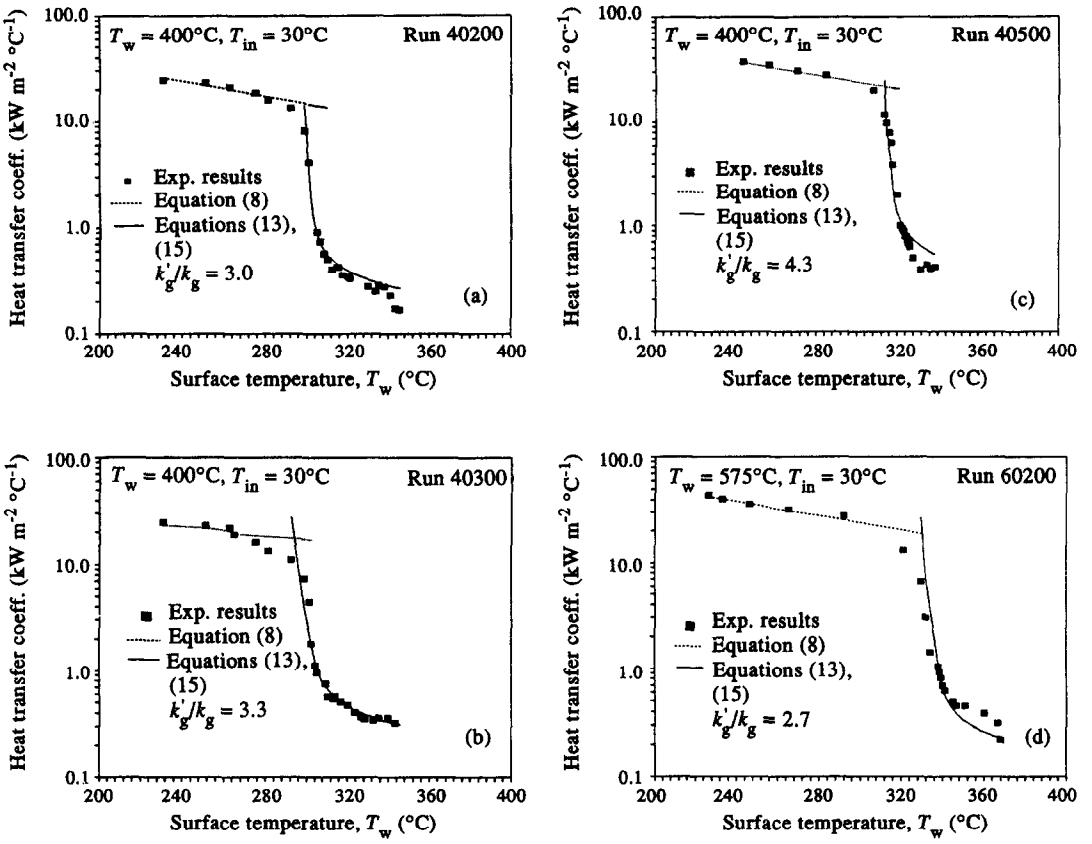

FIG. 10. Heat transfer coefficient vs surface temperature at the quench for different inlet and initial conditions.

For the present test conditions of low flow rate and low power, equation (8) compares well with measured data in region *B* (Fig. 10). At the high temperature end of this region and in region C, the heat flux drops dramatically with only slight change of the surface superheat. Downstream of region B (in regions C and D) heat transfer is mainly by forced convection to vapor and by boiling of liquid droplets impinging on the wall.

3.5. *Precursory cooling*

Precursory cooling refers here to the various modes of surface heat transfer taking place downstream of the quench front (regions C and D in Fig. 8). Region C, close to the quench front, in the temperature range $T_r < T_w < T_{AR}$, is characterized by large variations in the surface heat flux and surface temperature due to rapid buildup and evaporation of the liquid film at the wavy quench front. Heat transfer in this region is mainly by transition boiling. Further downstream, at higher wall temperatures (region D in Fig. 8), heat transfer is mainly by radiation and forced convection to the superheated vapor film which separates the heated wall from the subcooled bulk of water. Region D is generally referred to as subcooled inverted annular film boiling. Since the liquid bulk in this region is typically subcooled no vapor generation takes place in D. The vapor flowing downstream of the quench front can originate in region B and C only. Thus, proper prediction of the precursory cooling heat transfer requires the consideration of mass and energy balance over regions B, C and D. To this end we assume, for simplicity, that the quench front region consists of a thin liquid film having a uniform thickness $\bar{\mu}$, flowing near the heated wall, as shown schematically in Fig. 6. Quenching of the heated surface may be described as a continuous process in which this 'embryo' film evaporates and is continuously regenerated. The rate of evaporation basically defines the quenching rate, i.e. the rate at which the quench front moves along the heated surface. An energy balance over the wall and the film region near the quench front yields a mathematical relationship between the average film thickness, the quench front velocity, the wall temperature and the inlet fluid conditions [34].

$$\bar{\mu} = \frac{U_q}{U_{in} - U_q} \frac{(\rho C d)_w (T_r - T_s)}{\rho_l [h_{fg} + C_p \Delta T_{sub}]}. \quad (9)$$

In equation (9) the wall is assumed to be thin and at a uniform temperature and the vapor and liquid phases are assumed in equilibrium. Since the evaporated liquid layer is continuously regenerated, the process may be treated as quasi steady. Assuming that there exists a steady mass balance between the rate of evaporation of the thin liquid layer at the wall and the vapor flow rate in the vapor annulus of width δ, then

the vapor velocity downstream of the quench front may be calculated by

$$U_g = \left(\frac{\rho_l}{\rho_g}\right)\frac{\bar{\mu}(U_{in}-U_q)}{\delta} + U_q. \quad (10)$$

The vapor velocity is used to calculate the heat flux in regions C and D by direct solution of the energy equation in the vapor

$$U_g\frac{\partial T}{\partial z} = \alpha_g\frac{\partial^2 T}{\partial y^2} \quad (11)$$

with the following initial and boundary conditions:

$$T(z,0) = T_w$$
$$T(z,\delta) = T_s$$
$$T(0,y) = T_s. \quad (12)$$

Equations (11) and (12) were solved in ref. [35], yielding

$$q''_w = -k_g\frac{\partial T(z,0)}{\partial y}$$
$$= \frac{k_g(T_w-T_s)}{\delta}\left\{1+2\sum_{n=1}^{\infty}\exp-(n\pi)^2\frac{z}{\delta\, Pe_g}\right\} \quad (13)$$

where Pe_g is the vapor Peclet number ($Pe_g = U_g\delta/\alpha_g$). For the range of vapor velocities and δ measured in this study, the vapor flow is turbulent. The vapor conductivity, k_g, in equation (13) is then replaced by an effective value [36]

$$k'_g = k_g\left(1+\frac{Re_g - Re_{tr}}{Re_{tr}}\right)^{0.8} \quad (14)$$

where a transition vapor Reynolds number, $Re_{tr} = 500$, is used similar to the critical number typically used to determine the transition to turbulent film flow over a plate [37, p. 55].

The radiation heat flux in regions C and D is given by

$$q''_{rad} = \frac{\sigma\varepsilon_w\varepsilon_l}{\varepsilon_l+\varepsilon_w(1-\varepsilon_l)(r_1/r_2)}(T_w^4 - T_s^4) \quad (15)$$

where $\varepsilon_l = 0.95$ and for inconel-600 $\varepsilon_w = 0.8$. r_1 and r_2 are the inner and outer radius of the vapor film, respectively.

Heat transfer coefficients based on the total convective and radiative heat flux, equations (13)–(15) along with equation (8) are compared to data in Fig. 10. The theoretical predictions shown in Fig. 10 use the measured δ. The heat transfer coefficients are calculated as $(q''_w + q''_{rad})/(T_w - T_s)$. Good agreement with the data is demonstrated over the entire quench front region. Note that the heat transfer coefficient upstream of the quench front is not constant as is often assumed in conduction controlled rewetting models.

4. SUMMARY

Experimental and theoretical study of the heat and mass transfer characteristics, during the rewetting of a heated vertical surface with subcooled liquid, is presented. The experimental program covers the range of parameters applicable to the accident scenario of LOCA in research reactors. The results of the present study, for bottom reflooding of inconel-600 tube with subcooled water at atmospheric pressure, can be summarized as follows.

- The ratio between the quench front velocity, U_q, and the inlet liquid velocity, U_{in}, is constant, although U_q might change due to local pressure fluctuations. A mathematical relation is presented (equation (1)) which correlates U_q and U_{in} in terms of the initial and and inlet conditions.
- The rewetting temperature, T_r, may be described as an intermediate contact temperature between the surface at the apparent temperature, T_{AR}, and the water at T_l. T_r lies between the maximum heat flux temperature, T_{max}, and the minimum film boiling temperature.
- At the quench front, a small fraction of the liquid forms a thin layer in contact with the wall. The average thickness of the liquid layer is defined by the rate of heat transfer from the wall. The layer is continuously evaporated and regenerated at the wall. Since the liquid bulk at the quench front is typically subcooled, no further evaporation takes place downstream of the quench front until the liquid bulk temperature reaches saturation. The evaporation of the liquid layer is, therefore, the only source of vapor in the precursory cooling zone downstream of the quench front.
- Data evaluation indicates the existence of four heat transfer zones along the wall, defined by the hot surface temperature, as follows: forced convection in subcooled boiling liquid ($T_{IB} < T_w < T_{max}$), 'wet' transition boiling ($T_{max} < T_w < T_r$), 'dry' transition zone ($T_r < T_w < T_{AR}$) and subcooled IAF zone ($T_w > T_{AR}$). In the last zone, the liquid does not come in contact with the wall and heat transfer is by convection to vapor and by radiation to the subcooled liquid core. The heat transfer coefficient in the 'dry' zones was calculated by a convection–conduction model using an enhancement factor to account for turbulences due to the vapor flow.
- The vapor film thickness in the IAF zone is almost constant in the first 30 to 50 mm downstream of the quench front.
- The assumption, used in some theoretical models, of a step change in the heat transfer coefficient in the precursory cooling region, is proved to be unsatisfactory. It is demonstrated that the values of the continuous heat transfer coefficient in the quenching zone match a typical boiling curve where the various heat transfer zones are well defined.

REFERENCES

1. G. Yadigaroglu, The reflooding phase of the LOCA in PWRs, Part 1: Core heat transfer and fluid flow, *Nucl. Safety* **19**(1), 20–36 (1978).

2. E. Elias and G. Yadigaroglu, The reflooding phase of the LOCA in PWRs, Part 2: Rewetting and liquid entrainment, *Nucl. Safety* **19**(2), 160–175 (1978).
3. J. G. Collier, Heat transfer in the post burnout region and during quenching and reflooding. In *Handbook of Multiphase Systems* (Edited by G. Hetsroni). Hemisphere, Washington, DC (1982).
4. S. Olek, Analytical models for the rewetting of hot surfaces, Paul Scherrer Inst. (PSI) Report No. 17, Würenlingen and Villigen, Switzerland (1988).
5. R. S. Dougall and W. M. Rohsenow, Film boiling on the inside of vertical tubes with upward flow of the fluid at low quality, MIT Report, MIT-TR-9079-26 (1963).
6. N. Takenaka, K. Akagawa, T. Fujii and K. Nishida, Experimental study on flow pattern and heat transfer of inverted annular flow, *Nucl. Engng Design* **120,** 293–300 (1990).
7. M. Aritomi, A. Inoue, S. Aoki and K. Hanawa, Thermohydraulic behavior of inverted annular flow, *Nucl. Engng Design* **120,** 281–291 (1990).
8. P. Ottosen, Experimental and theoretical investigation of inverse annular film flow and dispersed droplet flow, important under LOCA conditions, RISO Nat'l Lab. Report, R-424, Denmark (1980).
9. M. Ishii and James P. Denten, Two-phase flow characteristic of inverted bubbly, slug and annular flow in post-critical heat flux region, *Nucl. Engng Design* **121,** 349–366 (1990).
10. J. Goodman and E. Elias, Heat transfer in the inverted annular flow regime during reflooding, *Trans. Am. Nucl. Soc.* **28,** 397 (1978).
11. Z. Edelman, E. Elias and D. Naot, Inverted annular boiling in a stainless-steel tube with steady heat sources, *Int. J. Heat Mass Transfer* **28**(7), 1281–1292 (1985).
12. Y. Barnea, E. Elias and I. Shai, Experimental apparatus for quantitative measurements in precursory cooling regime during bottom reflooding, *Trans. 22nd Israel Conf. on Mech. Engng*, p. 3.2.3 (1988).
13. Y. Barnea, E. Elias and I. Shai, Quantitative measurements in precursory cooling regime during bottom reflooding, *Trans. Israel Nucl. Soc.* **16,** 169 (1990).
14. Y. Koizumi, Y. Anoda, H. Kumamaru, T. Yonomoto and K. Tasaka, High-pressure reflooding experiments of multi-rod bundle at ROSA-IV TPTF, *Nucl. Engng Design* **120,** 301–310 (1990).
15. S. Muto, T. Anegawa, S. Morooka, S. Yokobori, Y. Takigawa, S. Ebata, Y. Yoshimoto and S. Suzuki, An experimental study on rewetting phenomena in transient conditions of BWRs, *Nucl. Engng Design* **120,** 311–321 (1990).
16. Y. Barnea, Precursory cooling during bottom reflooding of hot surfaces with subcooled liquid, D.Sc. Thesis, Technion—IIT (1991).
17. J. J. Carbajo and A. D. Siegel, Review and comparison among different models for rewetting in LWR's, *Nucl. Engng Design* **58,** 33–44 (1980).
18. S. Olek, Y. Zvirin and E. Elias, rewetting of hot surfaces by falling liquid films as a conjugate heat transfer problem, *Int. J. Multiphase Flow* **31**(1), 13–33 (1988).
19. B. D. G. Piggot and R. B. Duffey, The quenching of irradiated fuel pins, *Nucl. Engng Design* **32,** 182 (1975).
20. F. S. Gunnerson and T. R. Yackle, Quenching and rewetting of nuclear fuel rods, *Nucl. Technol.* **54,** 113–117 (1981).
21. R. A. Seban, S. T. Wang, C. L. La Jeunesse and A. Heydari, Heat transfer during quench and dryout in a vertical tube, EPRI Report NP-4157 (1985).
22. A. K. Kim and Y. Lee, A correlation of rewetting temperature, *Lett. Heat Mass Transfer* **6,** 117 (1979).
23. H. S. Carslaw and J. C. Jaeger, *Conduction of Heat in Solids* (2nd Edn). Claredon Press, Oxford (1959).
24. K. P. Yu, An experimental investigation of the reflooding of a bare tubular test section, Ph.D. Thesis, University of California, Berkeley (1978).
25. N. T. Obot and M. Ishii, Two-phase flow transition criteria post-dryout region based on flow visualization experiments, *Int. J Heat Mass Transfer* **31,** 2559 (1988).
26. P. L. Chambré and E. Elias, Rewetting model using a generalized boiling curve, EPRI Report NP-435 (1977).
27. J. G. Collier, *Convective Boiling and Condensation.* McGraw-Hill, London (1972).
28. A. E. Bergles and W. M. Rohsenow, The determination of forced convection surface boiling heat transfer, *Trans. ASME, J. Heat Transfer* **86,** 365 (1964).
29. P. Saha and N. Zuber, Point of net vapor generation and vapor void fraction in sub-cooled boiling, *Proc. 5th Int. Heat Transfer Conf.* **4,** B4.7, Tokyo (1974).
30. V. V. Klimenko, A generalized correlation for two-phase forced flow heat transfer—a second assessment, *Int. J. Heat Mass Transfer* **33,** 2073 (1990).
31. J. J. Carbajo, A study on rewetting temperature, *Nucl. Engng Design* **84,** 21 (1985).
32. G. Yadigaroglu, M. Andreani, S. N. Aksan, M. J. Lewis, G. Th. Analytis, D. Lübbesmeyer and S. Olek, Modelling of thermohydraulic emergency core cooling phenomena, PSI—Bericht Nr. 27, Paul Scherrer Institut (1990).
33. W. M. Rohsenow, A method of correlating heat transfer data for surface boiling liquids, *Trans. ASME J. Heat Transfer* **74,** 969 (1952).
34. Y. Barnea, E. Elias and I. Shai, Vapor generation rate at the quench front during inverted annular film boiling, *Proc. 4th Intern. Topical Meeting on Nucl. Reactor Thermal-Hydraulics*, Vol. **2,** pp. 1087–1091, Karlsruhe, F.R.G., 10–13 October (1989).
35. E. Elias and P. L. Chambré, Inverted-annular film boiling heat transfer from vertical surfaces, *Nucl. Engng Design* **64,** 249 (1981).
36. R. Seban *et al.*, Comparison of experimental and predicted heat transfer for the data of the UCB reflood experiment, EPRI Report NP-1290 (1979).
37. D. B. Spalding, *Convective Mass Transfer.* Edward Arnold, London (1963).